

## Article

# Catalysts Based on Ni(Mg)Al-Layered Hydroxides Prepared by Mechanical Activation for Furfural Hydrogenation

Liudmila N. Stepanova <sup>1,\*</sup>, Elena O. Kobzar <sup>1</sup>, Mikhail V. Trenikhin <sup>1</sup>, Natalia N. Leont'eva <sup>1</sup>, Aleksandra N. Serkova <sup>2</sup>, Aleksei N. Salanov <sup>2</sup> and Aleksandr V. Lavrenov <sup>1</sup>

<sup>1</sup> Center of New Chemical Technologies, Boreskov Institute of Catalysis, 54 Neftezhavodskaya Street, 644040 Omsk, Russia

<sup>2</sup> Boreskov Institute of Catalysis, 5 Acad. Lavrentieva Ave., 630090 Novosibirsk, Russia

\* Correspondence: lchem@yandex.ru

**Abstract:** Ni(Mg)Al-layered hydroxides with molar ratios of (Ni + Mg)/Al = 2, 3, 4 and Ni/(Ni + Mg) = 0.1, 0.3, 0.5, 0.7 were synthesized by mechanochemical activation. It has been proven that the phase composition of the samples was presented by a single hydrotalcite phase up to Ni/(Ni + Mg) = 0.5. For the first time, catalysts based on Ni(Mg)Al-layered hydroxides prepared by a mechanochemical route have been studied in the reaction of furfural hydrogenation. The correlation between furfural conversion, the selectivity of the products, and the composition of the catalysts was established. The effect of phase composition, surface morphology, and microstructure on the activity of the catalysts was shown by XRD, SEM, and TEM. It was found that catalysts with Ni/(Ni + Mg) = 0.5 have the highest furfural conversion. Herewith, the product selectivity can be regulated by the (Ni + Mg)/Al ratio.

**Keywords:** nickel; mixed oxides; mechanochemical synthesis; furfural hydrogenation; TEM



**Citation:** Stepanova, L.N.; Kobzar, E.O.; Trenikhin, M.V.; Leont'eva, N.N.; Serkova, A.N.; Salanov, A.N.; Lavrenov, A.V. Catalysts Based on Ni(Mg)Al-Layered Hydroxides Prepared by Mechanical Activation for Furfural Hydrogenation. *Catalysts* **2023**, *13*, 497. <https://doi.org/10.3390/catal13030497>

Academic Editors: Roman G. Kukushkin, Petr M. Yeletsky and Albert Poater

Received: 15 February 2023

Revised: 26 February 2023

Accepted: 27 February 2023

Published: 28 February 2023



**Copyright:** © 2023 by the authors. Licensee MDPI, Basel, Switzerland. This article is an open access article distributed under the terms and conditions of the Creative Commons Attribution (CC BY) license (<https://creativecommons.org/licenses/by/4.0/>).

## 1. Introduction

In recent years, much attention has been paid to the development of new possibilities for the production of fuel and chemicals from no-fossil carbon resources. Furfural (FAL) is a chemical obtained from lignocellulosic biomass, which is a renewable source. Due to the presence of an aldehyde group and a conjugated system of double bonds, FAL can go through several reactions, allowing the production of a range of value-added products [1,2]. FAL hydrogenation is a promising process that allows a number of industrially important compounds to be obtained. The most valuable products of FAL hydrogenation are furfuryl alcohol (FOL) and tetrahydrofurfuryl alcohol (THFOL). FOL is used mainly in the polymer industry together with the production of synthetic fibers, rubbers, resins, and farm chemicals, in the manufacture of lysine, vitamin C, and lubricants, the production of foundry sand binders in the metal casting industry, and as a chemical building block for drug synthesis. Moreover, FOL is also used in the production of other products in the fine chemical industry. THFOL, which is a deep-hydrogenation product of FAL, is an important green solvent used in agriculture and the printing industry [3,4].

There are two approaches for FAL hydrogenation: vapor-phase [5–7] and liquid-phase [8–10]. Vapor-phase hydrogenation of FAL is associated with issues related to catalyst deactivation due to coke formation, changes in oxidation states of active metals, and sintering of metal particles during the reaction. Additionally, selectivity for FOL is lower in the vapor-phase than the liquid-phase hydrogenation process [11,12]. Different organic compounds are used as solvents in liquid-phase furfural hydrogenation (ethanol, propanol, isopropanol, cyclopentyl methyl ether) [13–15]. However, these solvents often take part in the reaction, leading to the formation of undesirable products. Using water as solvent for the reaction of the liquid phase in this reaction has great advantages due to the non-toxicity and availability of water. Moreover, FAL is frequently obtained in the aqueous

solution in industry, and therefore the use of water as a solvent in its further transformations is the most economically competitive option, since it eliminates the expensive stage of separation of FAL–water systems [16,17]. However, most catalysts are not optimized to work under aqueous conditions and deactivation is significant because of strong water corrosion [18].

Different catalytic systems have been developing for both for vapor-phase and liquid-phase furfural hydrogenation [15,18]. Industrial copper-chromium catalysts have a high catalytic activity. However, the toxicity of chromium compounds limits their use. Catalysts with noble metals have good catalytic characteristics, but they have a high cost. Therefore, the search for new eco-friendly catalysts with high activity and adjustable selectivity continues.

The development of nickel-containing catalysts for the reaction of FAL hydrogenation is an intensively developing area [9,19–22]. The catalysts containing Ni on different supports ( $\text{SiO}_2$ ,  $\text{Al}_2\text{O}_3$ , mesoporous clays, carbon materials, Ni-based MOFs) have a sufficiently high activity in FAL hydrogenation and low cost. Additionally, they do not contain toxic substances. At the same time, the problems of an increase in dispersion and achieving balance between the acid-base properties of the catalysts for the decrease in coke formation remain unsolved for Ni-containing systems. Therefore, a search for new supports or methods for the synthesis of catalysts that partially or completely overcome these problems is necessary. Moreover, the simultaneous presence of the hydrogenation sites and Lewis acid sites may affect the catalytic hydrogen transfer. This has a significant impact on the selectivity of the obtained products [18].

Introduction of nickel in the composition of layer double hydroxides (LDHs) allows a high dispersion of hydrogenation metals to be achieved at the atomic level. It is possible due to the unique structure of these materials. It is a class of inorganic compounds with a general formula  $[\text{M(II)}_{1-x} \text{M(III)}_x(\text{OH})_2] \bullet [\text{A}^{n-}]_{x/n} \bullet m\text{H}_2\text{O}$ , where M(II) and M(III) are divalent and trivalent cations,  $\text{A}^{n-}$  is the anion, and  $x$  can generally have the values between 0.2 and 0.4 [23]. They have a positively charged brucite-like host matrix (comprising different metal cations) and exchangeable interlayer guest anions. The oxidation and reduction treatment of LDH precursors will give rise to supported metal nanoparticles on a mixed-metal oxide. Such materials demonstrated a high specific surface area, adjustable acid-base properties, and the possibility to control metal type, particle size, and metal–support interactions [4,24].

There are some research papers devoted to the study of Ni-containing oxides prepared from LDHs in the reactions of selective hydrogenation of furan compounds. At the same time, both systems containing only nickel as a hydrogenating metal [4,25–28] and systems containing promoter metals (Fe, Cu, Co, Mo, Pt, In) in their composition, which further improve the properties of nickel catalysts [29–37], were studied. In the presented papers, a high dispersion of Ni in the composition of the mixed oxide systems was pointed out. Authors noticed moderate acid-base properties of the Ni catalysts based on LDHs as an additional advantage. For example, in the reaction of hydroxymethylfurfural hydrogenation, acid sites tend to catalyze rearrangement and condensation to form humins, thereby lowering selectivity and causing carbon deposition on catalysts [26]. An excessive number of basic sites may induce a repulsive effect on the furan ring to adversely affect the ring hydrogenation [26,38]. Meanwhile, the acid and base properties of the Ni-containing catalysts prepared from LDHs could be tuned by its mole metals ratio. The catalysts demonstrated not only high activity and adjustable selectivity in the reaction but improved hydrothermal stability. This prevents the undesired agglomeration and leaching of Ni in the hydrothermal environment [26]. NiAl catalysts possessed this property due to enhanced metal support interactions that may be additionally increased by the introduction of Mg in the NiAl-LDH composition [25,26]. The data presented in the literature indicate a high capability of Ni-containing systems prepared from corresponding LDHs to be used as catalysts for the reaction of hydrogenation of furan compounds.

Coprecipitation is a traditional method of LDH synthesis [39]. However, it has a lot of disadvantages. The main ones are a large number of stages, duration, and the large amount of alkaline rinsing water. Mechanochemical synthesis is an alternative method of LDH preparation. In this method, the solid-phase reaction between initial reagents at the mechanical action occurs. As a result, transformation of mechanical energy into chemical energy is observed, and ultimately, this promotes the formation of a new compound. There is very limited information in the literature concerning the use of the mechanochemical method for the preparation of Ni-containing LDH [40,41]. Herewith, the data about the application of prepared systems as catalyst precursors for the reaction of FAL hydrogenation are not yet available. At the same time, the use of the mechanochemical method for Ni-containing LDH synthesis not only significantly speeds up the process and helps to reduce the amount of alkaline wash water but can change the properties of the systems due to the uniqueness of the processes occurring at mechanochemical activation.

The aim of this work was the synthesis of NiAl- and NiMgAl-layered hydroxides under mechanical impact and establishing a relationship between catalyst composition, Ni active site properties, and characteristics of corresponding catalysts in the reaction of aqua-phase FAL hydrogenation.

## 2. Results and Discussion

### 2.1. Study of Phase Composition and Morphology of as-Synthesized Ni(Mg)Al-Layered Hydroxides

In this work, the series of Ni-containing layered hydroxides with different (Ni + Mg)/Al and Ni/(Ni + Mg) molar ratios were synthesized by mechanochemical activation. Hydroxides NiAl-2 (Ni/Al = 2), NiAl-3 (Ni/Al = 3), and NiAl-4 (Ni/Al = 4) with two metals in composition were prepared. Additionally, hydroxides NiMgAl-2 (Ni/(Ni + Mg) = 0.1, 0.3, 0.5, 0.7; (Ni + Mg)/Al = 2), NiMgAl-3 (Ni/(Ni + Mg) = 0.3, 0.5; (Ni + Mg)/Al = 3), and NiMgAl-4 (Ni/(Ni + Mg) = 0.3, 0.5; (Ni + Mg)/Al = 4) were synthesized in a similar way. For comparison, MgAl-LDHs with different Mg/Al molar ratios were also prepared by the mechanochemical method.

According to XRD data for (Ni + Mg)/Al = 2 and Ni/(Ni + Mg) = 0.1, 0.3, and 0.5, the reflexes of the LDH phase are observed (Figure 1a). Peaks 003 and 006 are observed in the low angles area ( $2\theta = 5 \div 30^\circ$ ), reflections 012, 015, and 018 are in the area of medium angles ( $2\theta = 30 \div 55^\circ$ ), and peaks 110 and 113 are in the region of high angles ( $2\theta = 55 \div 80^\circ$ ). The increase in Ni/(Ni + Mg) from 0.5 to 1.0 leads to the decrease in the intensity of the LDH peaks. Moreover, the additional peaks at approximately  $18^\circ$  and  $38^\circ$  appeared. These peaks are attributed to gibbsite and theophrastrite. The increase in Ni content leads to a decrease in crystallinity of the samples. Also, there was no complete reaction between initial reagents as the Ni content increased. Therefore, the peaks of  $\text{Al}(\text{OH})_3$  and  $\text{Ni}(\text{OH})_2$  were in the XRD patterns of corresponding samples. A similar trend of changes in XRD patterns was observed for the samples with molar ratio of (Ni+Mg) = 3 and 4 (Figure 1b,c).

It is well known that the morphological characteristics of LDH are significantly affected by the cation composition and the synthesis conditions. According to obtained SEM data the morphology of NiAl-LDH prepared in this work by mechanochemical method was very similar irrespective of Ni/Al molar ratio (Figures 2 and S1). The surface morphology of NiAl-LDH is presented by agglomerated plate-like particles oriented in horizontal plane (Figure 2a–d). For the NiMgAl-LDH samples rounded plates become more distinguishable (Figure 2e–h). Areas with a relatively loose and relatively dense surface structure are found for the 0.3NiMgAl-4 sample (Figure 2g,h-insert). The morphology of 0.5NiMgAl-4 was most different from all the others. It presented by uniform nanostructure of rounded plate-like particles with the same shape and size of about 0.15 micrometers.

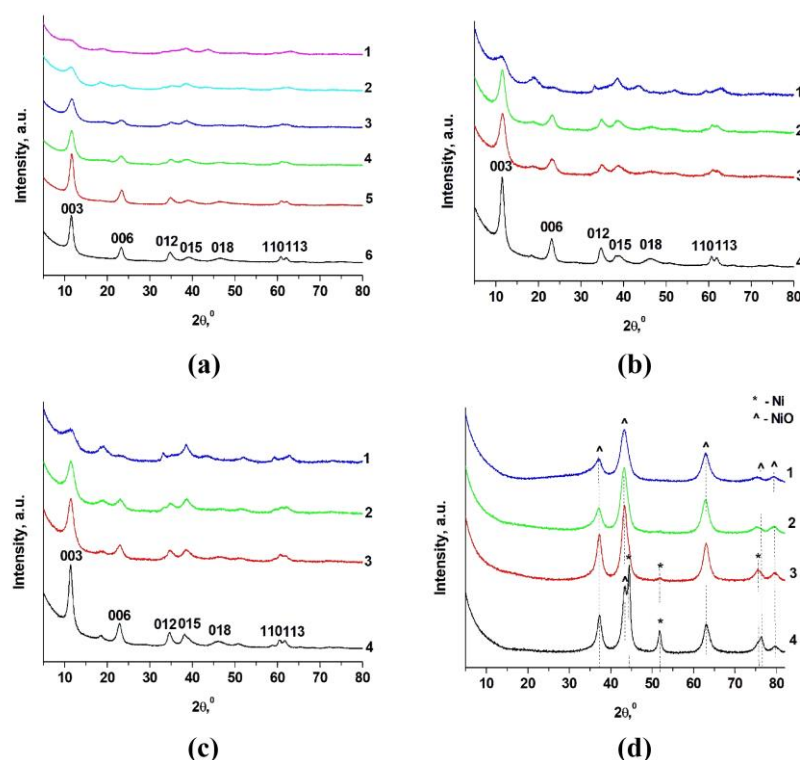


**Figure 1.** XRD patterns of the samples: (a)  $(\text{Ni} + \text{Mg})/\text{Al} = 2$ , 1-NiAl-2, 2-0.7NiMgAl-2, 3-0.5NiMgAl-2, 4-0.3NiMgAl-2, 5-0.1NiMgAl-2, 6-MgAl-2; (b)  $(\text{Ni} + \text{Mg})/\text{Al} = 3$ , 1-NiAl-3, 2-0.5NiMgAl-3, 3-0.3NiMgAl-3, 4-MgAl-3; (c)  $(\text{Ni} + \text{Mg})/\text{Al} = 4$ , 1-NiAl-4, 2-0.5NiMgAl-4, 3-0.3NiMgAl-4, 4-MgAl-4; (d) samples after calcination and reduction pretreatments: 1-0.5NiMgAl-2-R, 2-0.5NiMgAl-4-R, 3-NiAl-3-R, 4-NiAl-4-R.

The morphology of Ni-containing LDH prepared by the mechanochemical method was largely different from the samples with the same composition produced by traditional coprecipitation. In accordance with the earlier obtained data, for the Ni-containing samples with  $\text{Ni}/(\text{Ni} + \text{Mg}) = 0.3$  and  $0.5$  prepared by coprecipitation, the «rosette» morphology is formed. Only for NiAl-LDH the «rosette» morphology become less pronounced [42]. The formation of a «rosette» morphology while obtaining several LDHs by coprecipitation is explained by the equality of the pH of the synthesis and the point of zero charge of the LDH. The mechanochemical method assumes the course of a solid-phase reaction between initial reagents with the LDH precursor formation. Next, this precursor transforms to the LDH phase during aging in water [43]. Therefore, the morphology of the Ni-containing samples, apparently, is determined by nucleation and crystal growth of the LDH particles at both the mechanical activation stage (the first stage) and aging (the second stage).

## 2.2. Study of the Properties of Actives Sites of the Catalysts

The samples after calcination at  $550\text{ }^{\circ}\text{C}$  and reduction in  $\text{H}_2$  flow at  $600\text{ }^{\circ}\text{C}$  were studied in the reaction of furfural hydrogenation. According to obtained thermal analysis data, the weight loss did not occur above  $550\text{ }^{\circ}\text{C}$  (Figure S2). This indicates the complete decomposition of the initial hydroxides. Thus, the decomposition temperature for the Ni-containing layered hydroxides prepared by the mechanochemical method was consistent with the decomposition temperature of the most layered hydroxides synthesized by coprecipitation [23]. It was demonstrated earlier that the temperature of  $600\text{ }^{\circ}\text{C}$  was enough for a reduction of nickel to the metallic state for the NiAl-LDH prepared by coprecipitation [42,44]. Thus, the same temperature was chosen for the reduction of Ni-containing samples prepared by the mechanochemical route. Additionally, the use of a similar temperature pretreatment of the catalysts will allow for a comparison of their catalytic properties.

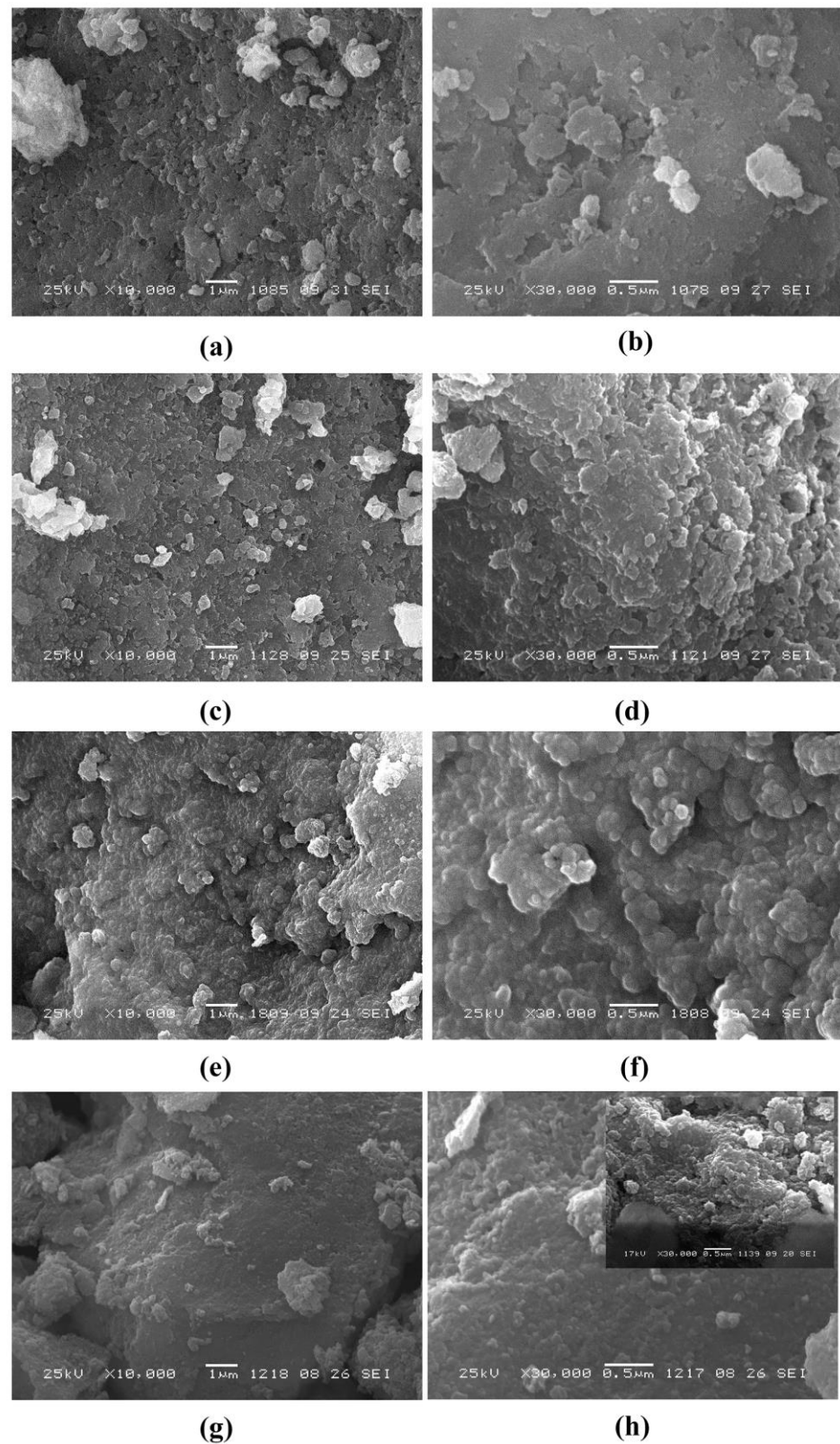


**Figure 2.** SEM images of the samples: (a,b) NiAl-3, (c,d) NiAl-4, 3, (e,f) 0.5NiMgAl-4, 4, (g,h) 0.3NiMgAl-4.

All the studied samples were active in the reaction of furfural hydrogenation. MgAl samples did not have any activity in the reaction. For the systems with  $(\text{Ni} + \text{Mg})/\text{Al} = 2$ , even at minor nickel content ( $\text{Ni}/(\text{Ni} + \text{Mg}) = 0.1$ ), the FAL conversion achieved 18%

(Figure 3a). The increase in Ni/(Ni + Mg) to 0.3 contributed to the full FAL conversion. The further increase in nickel content in the catalysts led to the decrease in their activity. Bimetallic NiAl-2-R catalyst had a value of FAL conversion of 53%. Thus, the dependent of FAL conversion from Ni/(Ni + Mg) molar ratio for the catalysts with (Ni + Mg)/Al = 2 had an extreme character with a maximum at Ni/(Ni + Mg) = 0.3. The products' selectivity and yield depended on Ni/(Ni + Mg) ratio, too (Table 1, Table S1). The samples with lower activity had a higher FOL selectivity (87–89%) and FOL yield (38–46%). The FOL selectivity was 40% and THFOL selectivity was 59% for 0.3Ni-MgAl-2-R. Moreover, a significant amount of THFAL (selectivity about 12.6%) was observed for the 0.3NiMgAl-2-R catalyst. Thus, the study of NiMgAl samples with Ni/(Ni + Mg) = 0.3 and 0.5 that had a higher activity in the reaction is of great interest. Therefore, these ratios of Ni/(Ni + Mg) were chosen for the synthesis by the mechanochemical method of the Ni-containing samples with (Ni + Mg)/Al = 3 and 4.

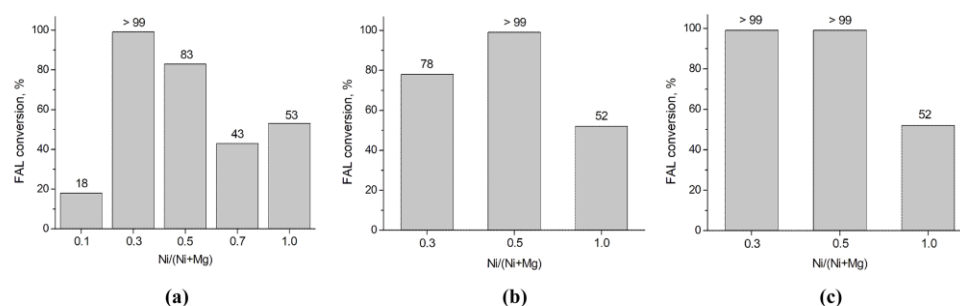


**Figure 3.** FAL conversion for the catalysts (a) (Ni + Mg)/Al = 2, (b) (Ni + Mg)/Al = 3, (c) (Ni + Mg)/Al = 4.

**Table 1.** Results of FAL hydrogenation in the presence of Ni(Mg)Al-R catalysts with different Ni/(Ni + Mg) and (Ni + Mg)/Al molar ratios (90 °C, 2.0 MPa, stirring 1400 rpm, reaction time 220 min).

Sample	(Ni + Mg)/Al	Ni/(Ni + Mg)	S, %			
			FOL	THFOL	THFAL *	Other Products
0.1NiMgAl-2-R	2	0.1	78	8	12.6	1.4
0.3NiMgAl-2-R		0.3	40	59	0.5	0.5
0.5NiMgAl-2-R		0.5	66	32	0.2	1.8
0.7NiMgAl-2-R		0.7	89	7	4.0	0.0
NiAl-2-R		1	87	9	4.0	0.0
0.3NiMgAl-3-R	3	0.3	50	32	17	1.0
0.5NiMgAl-3-R		0.5	39	61	0.0	0.0
NiAl-3-R		1	88	9	3.0	0.0
0.3NiMgAl-4-R	4	0.3	43	57	0.0	0.0
0.5NiMgAl-4-R		0.5	30	70	0.0	0.0
NiAl-4-R		1	87	7	4.7	1.3

\* tetrahydrofurfural.

NiAl-R had almost the same activity in the reaction irrespective of the Ni/Al molar ratio. At the same time, the FAL conversion did not exceed 53%. As for the systems with (Ni + Mg)/Al = 2, for the catalysts with a higher (Ni + Mg)/Al ratio the introduction of Mg in the composition led to a great increase in the activity of the catalysts (Figure 3b,c). For the catalysts with (Ni + Mg)/Al = 3, the highest activity (FAL conversion more than 99%) was observed for the sample with Ni/(Ni + Mg) = 0.5. The full FAL conversion was achieved for the studied NiMgAl catalysts with (Ni + Mg)/Al = 4. The trend of selectivity change for the catalysts with (Ni + Mg)/Al = 3 and 4 was the same as for the systems with (Ni + Mg)/Al = 2. The FOL selectivity and FOL yield decreased with an increase in FAL

conversion. Herewith, for the catalysts with  $(\text{Ni} + \text{Mg})/\text{Al} = 4$  that were characterized by full FAL conversion, the THFOL selectivity rose with the increase in  $\text{Ni}/(\text{Ni} + \text{Al})$  ratio and achieved 70% for the 0.5NiMgAl-4-R. The THFOL yield was 69.4% for this catalyst (Table S1).

It is possible to make the following intermediate conclusions in accordance with the obtained catalytic data. The catalysts that contained only Ni and Al in the composition (NiAl-2-R, NiAl-3-R, NiAl-4-R) showed almost the same activity in the reaction of FAL hydrogenation (FAL conversion 52–53%, FOL selectivity 87–88%). Introduction of Mg in the composition of the catalysts facilitated a significant improvement of their catalytic characteristics. At the same time, the samples with  $\text{Ni}/(\text{Ni} + \text{Mg}) = 0.3$  and 0.5 had the best catalytic properties.

It is well known that the composition of active sites, their dispersion (size), and availability for the reactants have a great impact on the catalytic properties of the samples in the hydrogenation reactions [45]. Thus, for the explanation of obtained regularities, the NiAl-3-R, NiAl-4-R, 0.5NiMgAl-2-R, and 0.5NiMgAl-4-R were chosen for detailed study by XRD and TEM. As has been mentioned above, NiAl-3-R and NiAl-4-R had the same catalytic properties. 0.5NiMgAl-2-R and 0.5NiMgAl-4-R had a much higher activity compared to NiAl catalysts. However, product selectivity was very different for these samples. Therefore, these systems were chosen for further study.

After consecutive calcination and reduction stages the vanishment of LDH reflections is observed on XRD patterns for all studied samples (Figure 1d). This indicates the total collapse of LDH layers. During calcination, the removal of interlayer water, the dehydroxylation of the lattices, and the decomposition of interlayer anions occurred (Figure S2) [23]. The broad reflections located at ca.  $37$ ,  $43$ , and  $63^\circ$   $2\theta$  in the XRD pattern of the sample appeared. They are adjacent to the (111), (200), and (220) facets of face-centered cubic NiO, respectively. Similar results have already been obtained for Ni-containing materials prepared from LDH that were synthesized by coprecipitation [42,44,46]. These peaks refer to the formation of a weakly crystalline mixed oxide  $\text{Ni}(\text{Mg})\text{AlO}_x$  phase with an  $\text{Al}^{3+}$ - or  $\text{Mg}^{2+}$ -doped NiO structure. For NiAl-2-R and NiAl-3-R, additional peaks at  $45$ ,  $52$ , and  $76^\circ$   $2\theta$  were presented on the XRD patterns. They can be assigned to reflections of the (111), (200), and (220) planes of face-centered cubic lattice for metallic nickel, respectively. The intensity of peaks related to  $\text{Ni}^0$  increased with the increase in the  $\text{Ni}/\text{Al}$  molar ratio (i.e., with increasing nickel content in the catalysts). It is interesting that there were no peaks ascribed to the metallic nickel on XRD patterns of the 0.5NiMgAl-2-R and 0.5NiMgAl-4-R. A similar situation was observed for NiAl catalysts prepared by coprecipitation and exposed high temperature treatment in  $\text{N}_2$  [47]. According to data from multiple studies in the literature, the temperature of  $600^\circ\text{C}$  is sufficient for the reduction of the main part of nickel in the materials based on NiAl-LDH [44,46,48]. One of the possible reasons for the absence of metallic Ni peaks at XRD patterns is their high dispersion. However, in the case of Ni-containing catalysts obtained from Ni-LDH there may be other reasons, which will be discussed below.

According to the obtained TEM images, the agglomerates of well-dispersed particles on the support were observed for all studied catalysts (Figure 4). They appeared as a cluster of irregular dark areas against the background of a lighter field of support. The number of areas containing agglomerates increased in the line 0.5NiMgAl-2-R, 0.5NiMgAl-4-R, NiAl-3-R, then NiAl-4-R, i.e., with increasing Ni content in the samples. Moreover, the agglomerates size rose as the nickel content increased in the catalysts, too. In accordance with microscopic data, the estimation of agglomerates size was completed. The particles of various sizes were in all studied catalysts. More uniform particle size distribution was presented for 0.5NiMgAl-2-R. The majority of agglomerates had the size about 4 nm, although particles with higher sizes of about 7.5 nm were in the sample, too. The particle size distribution became less homogeneous with the increase in Ni content in the samples. The average agglomerates size rose for the 0.5NiMgAl-4-R to 6.5 nm (with some part of the particles with sizes of about 11 nm). For NiAl-3-R, areas with agglomerates with

average sizes of 5, 7.5, and 14.5 nm were observed. For the sample with higher Ni content (NiAl-4-R), a small proportion of agglomerates with sizes of about 8 nm was presented. However, the majority of agglomerates had very different sizes (10–28 nm) with an average value of 17 nm.

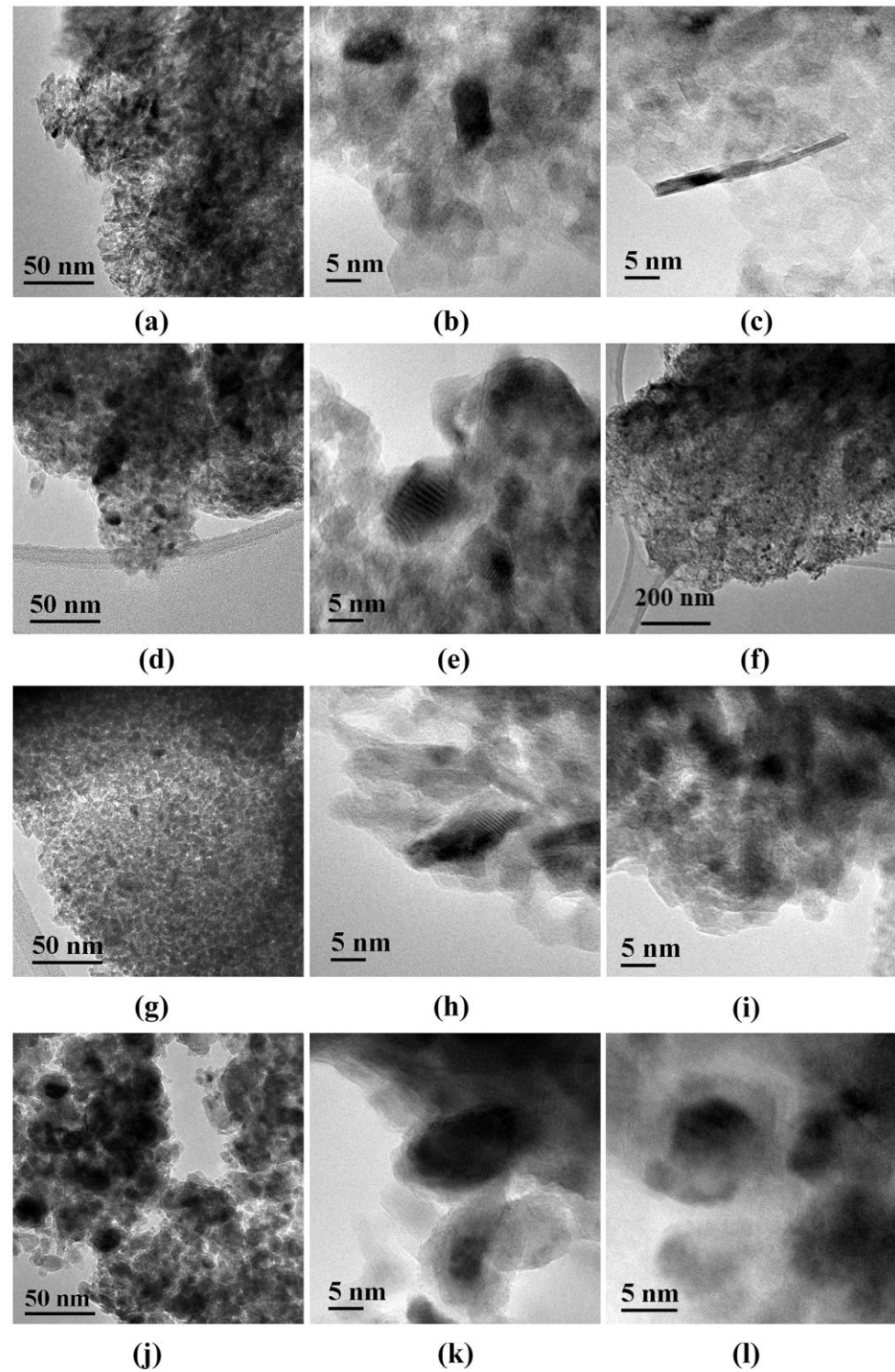


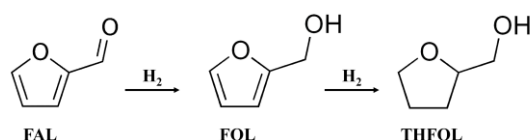
**Figure 4.** TEM images for the catalysts: (a–c) 0.5NiMgAl-2-R, (d–f) 0.5NiMgAl-4-R, (g–i) NiAl-3-R, (j–l) NiAl-4-R.

Different areas of the catalysts showed a lattice fringe of 0.243 nm that was assigned to the planes of multiple Ni(Mg)Al-mixed oxides. The abundant ambiguous lattices indicate low crystallinity of the oxides, and this is in full compliance with XRD data. Additionally, there were many areas with lattice fringes of 0.208 nm for NiAl-4-Red. This may be due to NiO formation during high temperature treatment for the sample with the highest Ni content. Despite the existence of metallic Ni in the NiAl-3-R and NiAl-4-R samples in accordance with XRD (Figure 1d), lattice fringes of Ni<sup>0</sup> were not detected by TEM for any of the studied samples. The crystal lattice was not allowed on the dark areas of the micrographs, which could obviously be attributed to metallic nickel. This was typical for both large agglomerates in NiAl-3-R (Figure 4g–i) and NiAl-4-R (Figure 4j–l), and smaller agglomerates in 0.5NiMgAl-2-R (Figure 4a–c) and 0.5NiMgAl-4-R (Figure 4d–f). The similar phenomenon was observed for some NiAl catalysts based on the corresponding LDH [47]. Only the STEM technique allowed the metallic nickel particles to be found. The superposition of the mixed oxides matrix and metallic nickel matrix allowed us to conclude that metal Ni clusters are implanted in the weakly crystalline Ni(Al)O<sub>x</sub> matrix. Moreover, it is possible to segregate Ni clusters inside the Ni(Al)O<sub>x</sub> matrix as the particles grow during reduction from the mixed oxide structure [46]. This can lead to the enrichment of Ni at the center of particles and formation of the Ni (core)/Ni(Al)O<sub>x</sub> (shell)/AlO<sub>x</sub> structure. Ni nanoparticles confined in the weakly crystalline Ni(Al)O<sub>x</sub> internal shell are embedded in amorphous AlO<sub>x</sub> networks. The authors managed to draw such conclusions based on the results of STEM-EDX. Cherepanova et al. [49] have demonstrated the formation of a sandwich-like structure for calcined NiAl-LDH prepared by coprecipitation. This structure consisted of a core with an Al-doped NiO-like structure and some surface layers with a spinel NiAl<sub>2</sub>O<sub>4</sub> structure epitaxial connected with the core. The mechanochemical method used in this work for the preparation of Ni-containing layered hydroxides leads to obtaining the materials comprising the particles with irregular morphology and agglomerations (macro level) and substantial lattice distortion and structure faults (in microcosm) [50]. Therefore, with a high degree of probability, it is possible to assume the formation of structures similar to those described in [46] for the obtained systems. Therefore, it is likely that the dark spots on the TEM images for the samples studied in this work correspond to metallic nickel. An additional confirmation of this is the increase in the number and size of these regions with an increase in the nickel content in the catalysts.

As has been shown in [29], the matrix of Ni(Al)O<sub>x</sub> facilitated better Ni dispersion. It explained the good catalytic activity (FAL conversion 52–53 wt. %) of the NiAl-3-R and NiAl-4-R catalysts with high Ni agglomerates (Figure 4g,j). The same and large size of agglomerates in these catalysts due to the high nickel content (Figure 3h–l) explain their similar catalytic properties in the reaction of FAL hydrogenation.

The introduction of magnesium to the catalyst composition additionally facilitated better Ni dispersion during mixed oxide formation [26]. It led to the formation of Ni particles with smaller sizes and as a consequence increased its activity in the reaction (Table 1, Figure 3a–f). Moreover, the NiO phase was presented in the samples NiAl-3-R and NiAl-4-R (Figures 1d and 4g,k,l). This phase could affect the catalysts' characteristics, because the oxidation state of the active metals in the catalyst will influence the activity and selectivity through promoting reactant activation and regulating the adsorption of intermediates [51,52]. The higher FAL conversion for the 0.5NiMgAl-4-R is explained by the higher content of highly dispersed Ni in the catalyst composition (Figure 4f).

The different product selectivity of the 0.5NiMgAl-2-R and 0.5NiMgAl-4-R catalysts can be explained from two points of view. The first explanation is based on the assumption of consistent products transformation during FAL hydrogenation (Scheme 1).



**Scheme 1.** Furfural transformation during hydrogenation process.

In this case, the higher FOL selectivity for 0.5NiMgAl-2-R is explained by the insufficient quantity of active nickel sites for the transformation of FOL to THFOL. The second explanation is connected with the assumption of different surface microstructures of studied catalysts. The authors of [4] found that catalysts prepared based on NiAl-LDH with NO<sub>3</sub> interlayer anions exhibited a high selectivity (97%) to FOL. At the same time, the samples synthesized from NiAl-LDH with CO<sub>3</sub> anions in the interlayer space showed an exclusive selectivity (99%) toward THFOL. A combination study allowed the authors to prove the existence of highly exposed Ni(111) planes on the CO<sub>3</sub>-based catalysts and multiplanes with abundant steps/vacancies for NO<sub>3</sub>-based systems. As a result, a large proportion of steps/edges of Ni nanoparticles in NO<sub>3</sub>-based catalysts suppressed the adsorption of the furan ring and only facilitated activated adsorption of the C=O group. In contrast, a high exposure of the Ni(111) plane in CO<sub>3</sub>-based catalysts promotes activated adsorption of both furan ring and C=O group, resulting in the production of THFOL. Different surface microstructures are not excluded for the samples obtained in this work. So, for a sample 0.5NiMgAl-2-R (Figure 4c), there are extended dark areas that are absent for the sample 0.5NiMgAl-4-R. However, this assumption requires additional study, which is beyond the scope of this work.

It is interesting to note that the similar surface morphology (according to SEM data) of NiAl samples affected by their similar catalytic properties, and different surface morphology of NiMgAl-LDH led to their higher activity and different selectivity.

Ni-containing catalysts based on LDH synthesized by coprecipitation have already been studied in our previous work [42]. For all prepared catalysts (NiAl-3-R, 0.3NiMgAl-3-R, 0.5NiMgAl-3-R), the distinct metallic Ni particles were observed on TEM images. Apparently, in the samples obtained by coprecipitation, nickel particles are less embedded in the oxide structure after high temperature treatments. Therefore, they are more accessible and better defined by TEM. At the same time, the trends in the catalytic properties of the samples obtained by coprecipitation, as well as the values of FAL conversion and product selectivity, were close to the samples obtained by the mechanochemical route.

### 3. Materials and Methods

#### 3.1. Catalysts Preparation

NiAl- and NiMgAl-LDH were prepared by the mechanochemical route. All initial reagents were taken from Omskreactive, Omsk, Russia. At the first stage, the mixture of dry initial reagents (Ni(OH)<sub>2</sub>, Al(OH)<sub>3</sub>, and Na<sub>2</sub>CO<sub>3</sub> for NiAl-LDH preparation and Ni(OH)<sub>2</sub>, Mg(OH)<sub>2</sub>, Al(OH)<sub>3</sub>, and Na<sub>2</sub>CO<sub>3</sub> for NiMgAl-LDH preparation) with desired ratios of metal cations was mechanically activated on a high-energy ball centrifugal planetary mill AGO-2. Mechanical activation was conducted in steel drums with steel milling bodies (d = 8 mm, acceleration = 1000 m s<sup>-2</sup>, the ratio of the mass of the reagents to the mass of the milling bodies = 1:20) for 30 min. At the second stage, the aging of the samples obtained after mechanical activation, in distilled water excess at constant stirring at 60 °C for 2 h, was carried out. Next, the samples were filtered and dried in air at 120 °C for 2 h. The obtained samples were denoted as NiAl-X or YNiMgAl-X, where X—molar ratio Ni/Al or (Ni + Mg)/Al, Y—molar ratio Ni/(Ni + Mg). For the preparation of the mixed oxides, the corresponding Ni-containing hydroxides were calcined at 550 °C. The final catalysts were produced by the reduction of corresponding mixed oxides in hydrogen flow at 600 °C for 2 h. The reduced samples were denoted as NiAl-X-R or YNiMgAl-X-R.

### 3.2. Catalysts Characterization

Structural properties of as-prepared NiAl- and NiMgAl-LDH and final catalysts (after oxidation and reduction stages) were studied by X-ray diffraction analysis (XRD). X-ray diffraction studies were carried out on a D8 Advance (Bruker, Billerica, MA, USA) diffractometer using Cu-K $\alpha$  source in the 2 $\theta$  angular range from 5° to 80°. The scanning step was 0.02°, and the signal integration time was 5 s/step. The phase composition of samples was identified using the international diffraction database ICDD PDF-2.

The surface morphology of the samples was investigated by using scanning electron microscopy (SEM) on a JSM-6460 LV (JEOL, Tokyo, Japan) instrument equipped with a tungsten cathode and working at an accelerating voltage of 20 kV. Before each experiment, the samples were ground in an agate mortar and fixed on a conducting double-sided carbon Scotch tape. To prevent the re-charging effects, a conducting gold film was sputtered on the fixed samples. Before each experiment, the samples were evacuated in the microscope chamber for 15–20 min to remove volatile compounds from the surface, which could exert a detrimental effect on the secondary electron emission and thus deteriorate quality of the image.

Thermal analysis (TG/DTA and DTG) was carried out using a DTG-60 (Shimadzu, Kyoto, Japan) instrument in the air atmosphere from room temperature to 700 °C at a heating rate of 10 °C min<sup>-1</sup>.

Transmission electron microscopy (TEM) images were obtained using a JEM-2100 electron microscope (JEOL Ltd, Tokyo, Japan) with a crystal lattice resolution of 0.14 nm and an accelerating voltage of 200 kV. The analysis and computer processing of electron microscopic images were performed using the Digital Micrograph "Gatan" program, as well as the Fast Fourier Transform (FFT) technique.

### 3.3. Catalysts Testing

For the liquid-phase reaction of hydrogenation of furfural, catalysts Ni(Mg)(A)IO<sub>x</sub> (500 mg) that were preliminarily oxidized and reduced in a stream of hydrogen (600 °C) were placed in a steel autoclave with a capacity of 180 ml together with distilled water (40 ml). To remove air components from the pore space of the catalyst, it was prereduced with hydrogen (T = 90 °C, pressure 2.0 MPa, stirring 1400 rpm, time 30 min) directly in the autoclave. The reaction mixture was heated to a predetermined temperature by circulating heated water through an external "jacket". After this activation, 5 mL of furfural and 60 mL of distilled water were placed in an autoclave. The furfural hydrogenation reaction was carried out at a temperature of 90 °C, a pressure of 2.0 MPa, with stirring at 1400 rpm. The reaction was controlled by measuring the volume of consumed hydrogen with a mass flow meter. The volume of consumed hydrogen normalized to normal conditions was recalculated to its equivalent amount that is needed for the formation of furfuryl alcohol from furfural. After completion of the reaction and cooling, the aqueous phase was separated from the catalyst by filtering. The quantitative determination of the reaction products was carried out by gas chromatography (Chromos GX-1000) in a capillary column VB-WAX (60 m × 0.32 mm) and a flame ionization detector.

The FAL conversion *X* (mol. %), selectivity to each product *S* (mol. %), and product yield *Y* (mol. %) were calculated as follows:

$$X = \frac{\text{moles of reacted FAL}}{\text{moles of initial FAL}} \cdot 100\% \quad (1)$$

$$S = \frac{\text{moles of product obtained}}{\text{moles of reacted FAL}} \cdot 100\% \quad (2)$$

$$Y = \frac{\text{moles of product obtained}}{\text{moles of initial FAL}} \cdot 100\% \quad (3)$$

#### 4. Conclusions

In the present work, Ni(Mg)Al-layered hydroxides with different (Ni + Mg)/Al and Ni/(Ni + Mg) molar ratios were synthesized by the mechanochemical method. Phase composition of the samples was presented by a single hydrotalcite phase up to Ni/(Ni + Mg) = 0.5. The composition of the samples with higher Ni/(Ni + Mg) were presented by additional gibbsite and theophorite phases. For the first time, properties of the catalysts obtained after high-temperature treatment of corresponding Ni(Mg)Al-LDH were studied in the reaction of furfural hydrogenation. It was found that NiAl catalysts had the same catalytic properties (FAL conversion 52–53%, FOL selectivity 87–88%). The best catalytic results were achieved by using NiMgAl catalysts with Ni/(Ni + Mg) = 0.3 and 0.5. The FAL selectivity of FOL formation increased with the increasing (Ni + Mg)/Al ratio. The same catalytic properties of NiAl catalysts can be explained by their close morphology and surface microstructure (the same size of active sites, their relatively large size). NiMgAl samples are characterized by the highly dispersed Ni with a lower size compared to the NiAl systems. The catalytic properties of studied catalysts did not exceed the catalytic properties of the catalysts with the same composition prepared by coprecipitation. Therefore, this paper shows the possibility of obtaining catalysts for furfural hydrogenation with excellent properties by using an eco-friendly synthesis procedure. The possibility of microstructural changes to catalysts by varying (Ni + Mg)/Al and Ni/(Ni + Mg) open new promising avenues for further research.

**Supplementary Materials:** The following supporting information can be downloaded at <https://www.mdpi.com/article/10.3390/catal13030497/s1>, Figure S1: SEM images of the samples: 1 (a,b)—NiAl-3; 2 (a,b)—NiAl-4; 3 (a,b)—0.5NiMgAl-4; 4 (a,b)—0.3NiMgAl-4; Figure S2. Curves of TG (red line), DrTG (black line), DTA (green line) of the samples: a—NiAl-4; b—0.3NiMgAl-4. Table S1. Yield of products of the reaction of FAL hydrogenation in the presence of Ni(Mg)Al-R catalysts with different Ni/(Ni+Mg) and (Ni+Mg)/Al molar ratio (90 °C, 2.0 MPa, stirring 1400 rpm, reaction time 220 min).

**Author Contributions:** L.N.S. conceptualization, writing—original draft preparation, writing—review and editing, methodology; E.O.K. investigation, writing—original draft preparation; M.V.T. investigation; N.N.L. investigation; A.N.S. (Aleksandra N. Serkova) investigation; A.N.S. (Aleksei N. Salanov) investigation; A.V.L. supervision. All authors have read and agreed to the published version of the manuscript.

**Funding:** This work was supported by the Ministry of Science and Higher Education of the Russian Federation within the governmental order for Boreskov Institute of Catalysis (project AAAA-A21-121011890074-4).

**Data Availability Statement:** Not applicable.

**Acknowledgments:** The authors are grateful to I.V. Muromtsev for the XRD experiments, A.V. Vasilevich for the TA experiments, and O.B. Belskaya for help at certain stages of the work. The study was carried out using the facilities of the shared research center “National center of investigation of catalysts” at Boreskov Institute of Catalysis. Analysis of the physicochemical properties of the samples was performed using the equipment of the “National Center for Catalyst Research” and the Omsk Regional Center for Collective Use of the Siberian Branch of the Russian Academy of Sciences.

**Conflicts of Interest:** The authors declare no conflict of interest.

#### References

1. Peleteiro, S.; Rivas, S.; Alonso, J.L.; Santos, V.; Parajó, J.C. Furfural production using ionic liquids: A review. *Bioresour. Technol.* **2016**, *202*, 181–191. [[CrossRef](#)] [[PubMed](#)]
2. Cai, C.M.; Zhang, T.; Kumar, R.; Wyman, C.E. Integrated furfural production as a renewable fuel and chemical platform from lignocellulosic biomass. *J. Chem. Technol. Biotechnol.* **2013**, *89*, 2–10. [[CrossRef](#)]
3. O’Driscoll, Á.; Leahy, J.J.; Curtin, T. The influence of metal selection on catalyst activity for the liquid phase hydrogenation of furfural to furfuryl alcohol. *Catal. Today* **2017**, *279*, 194–201. [[CrossRef](#)]
4. Meng, X.; Yang, Y.; Chen, L.; Xu, M.; Zhang, X.; Wei, M. A Control over Hydrogenation Selectivity of Furfural via Tuning Exposed Facet of Ni Catalysts. *ACS Catal.* **2019**, *9*, 4226–4235. [[CrossRef](#)]

5. Seo, G.; Chon, H. Hydrogenation of furfural over copper-containing catalysts. *J. Catal.* **1981**, *67*, 424–429. [[CrossRef](#)]
6. Prakruthi, H.R.; Chandrashekhara, B.M.; Prakash, J.; Bhat, Y.S. Hydrogenation efficiency of highly porous Cu-Al oxides derived from dealuminated LDH in the conversion of furfural to furfuryl alcohol. *Ind. Eng. Chem. Res.* **2018**, *62*, 96–105. [[CrossRef](#)]
7. Jiménez-Gómez, C.P.; Cecilia, J.A.; Franco-Duro, F.I.; Pozo, M.; Moreno-Tost, R.; Maireles-Torres, P. Promotion effect of Ce or Zn oxides for improving furfuryl alcohol yield in the furfural hydrogenation using inexpensive Cu-based catalysts. *J. Mol. Catal.* **2018**, *455*, 121–131. [[CrossRef](#)]
8. Liu, L.; Lou, H.; Chen, M. Selective hydrogenation of furfural over Pt based and Pd based bimetallic catalysts supported on modified multiwalled carbon nanotubes (MWNT). *Appl. Catal. A Gen.* **2018**, *550*, 1–10. [[CrossRef](#)]
9. Gong, W.; Chen, C.; Wang, H.; Fan, R.; Zhang, H.; Wang, G.; Zhao, H. Sulfonate group modified Ni catalyst for highly efficient liquid-phase selective hydrogenation of bio-derived furfural. *Chin. Chem. Lett.* **2018**, *29*, 1617–1620. [[CrossRef](#)]
10. Nguyen-Huy, C.; Kim, J.S.; Yoon, S.; Yang, E.; Kwak, J.H.; Lee, M.S.; An, K. Supported Pd nanoparticle catalysts with high activities and selectivities in liquid-phase furfural hydrogenation. *Fuel* **2018**, *226*, 607–617. [[CrossRef](#)]
11. Bhogeswararao, S.; Srinivas, D. Catalytic conversion of furfural to industrial chemicals over supported Pt and Pd catalysts. *J. Catal.* **2015**, *327*, 65–77. [[CrossRef](#)]
12. Rao, R.; Dandekar, A.; Baker, R.T.K.; Vannice, M.A. Properties of copper chromite catalysts in hydrogenation reactions. *J. Catal.* **1997**, *171*, 406–419. [[CrossRef](#)]
13. Gupta, K.; Rai, R.K.; Singh, S.K. Metal catalysts for Efficient transformation of biomass-derived HMF and furfural to value added chemicals: Recent progress. *ChemCatChem.* **2018**, *10*, 2326–2349. [[CrossRef](#)]
14. Yang, X.; Meng, Q.; Ding, G.; Wang, Y.; Chena, H.; Zhu, Y.; Li, Y.W. Construction of novel Cu/ZnO-Al<sub>2</sub>O<sub>3</sub> composites for furfural hydrogenation: The role of Al components. *Appl. Catal. A Gen.* **2018**, *561*, 78–86. [[CrossRef](#)]
15. Wang, Y.; Zhao, D.; Rodríguez-Padrón, D.; Len, C. Recent advances in catalytic hydrogenation of furfural. *Catalysts* **2019**, *9*, 796. [[CrossRef](#)]
16. Musci, J.J.; Merlo, A.B.; Casella, M.L. Aqueous phase hydrogenation of furfural using carbon-supported Ru and RuSn catalysts. *Catal. Today* **2017**, *296*, 43–50. [[CrossRef](#)]
17. Mika, L.T.; Cséfalvay, E.; Horváth, I.T. The role of water in catalytic biomass-based technologies to produce chemicals and fuels. *Catal. Today* **2015**, *247*, 33–46. [[CrossRef](#)]
18. Wu, K.; Wu, Y.; Chen, Y.; Chen, H.; Wang, J.; Yang, M. Heterogeneous catalytic conversion of biobased chemicals into liquid Fuels in the aqueous phase. *ChemSusChem* **2016**, *9*, 1355–1385. [[CrossRef](#)]
19. Sunyol, C.; English Owen, R.; González, M.D.; Salagre, P.; Cesteros, Y. Catalytic hydrogenation of furfural to tetrahydrofurfuryl alcohol using competitive nickel catalysts supported on mesoporous clays. *Appl. Catal. A Gen.* **2021**, *611*, 117903. [[CrossRef](#)]
20. Gao, G.; Shao, Y.; Gao, Y.; Wei, T.; Gao, G.; Zhang, S.; Wang, Y.; Chen, Q.; Hu, X. Synergetic effects of hydrogenation and acidic sites in phosphorus-modified nickel catalysts for the selective conversion of furfural to cyclopentanone. *Catal. Sci. Technol.* **2021**, *11*, 575–593. [[CrossRef](#)]
21. Gong, W.; Chen, C.; Zhang, H.; Zhang, Y.; Zhang, Y.; Wang, G.; Zhao, H. Highly selective liquid-phase hydrogenation of furfural over N-doped carbon supported metallic nickel catalyst under mild conditions. *J. Mol. Catal. A Chem.* **2017**, *429*, 51–59. [[CrossRef](#)]
22. Guo, P.; Liao, S.; Tong, X. Heterogeneous Nickel Catalysts Derived from 2D Metal–Organic Frameworks for Regulating the Selectivity of Furfural Hydrogenation. *ACS Omega* **2019**, *4*, 21724–21731. [[CrossRef](#)] [[PubMed](#)]
23. Cavani, F.; Trifirò, F.; Vaccari, A. Hydrotalcite-type anionic clays: Preparation, properties and applications. *Catal. Today* **1991**, *11*, 173–301. [[CrossRef](#)]
24. Yamaguchi, K.; Ebitani, K.; Yoshida, T.; Yoshida, H.; Kaneda, K. Mg–Al mixed oxides as highly active acid–Base catalysts for cycloaddition of carbon dioxide to epoxides. *J. Am. Chem. Soc.* **1999**, *121*, 4526–4527. [[CrossRef](#)]
25. Sulmonetti, T.P.; Pang, S.H.; Claire, M.T.; Lee, S.; Cullen, D.A.; Agrawal, P.K.; Jones, C.W. Vapor phase hydrogenation of furfural over nickel mixed metal oxide catalysts derived from layered double hydroxides. *Appl. Catal. A Gen.* **2016**, *517*, 187–195. [[CrossRef](#)]
26. Zhong, F.; Ge, X.; Sun, W.; Du, W.; Sang, K.; Yao, C.; Cao, Y.; Chen, W.; Qian, G.; Duan, X.; et al. Total hydrogenation of hydroxymethylfurfural via hydrothermally stable Ni catalysts and the mechanistic study. *Chem. Eng. J.* **2023**, *455*, 140536. [[CrossRef](#)]
27. Song, Y.; Beaumont, S.; Zhang, X.; Wilson, K.; Lee, A.F. Catalytic applications of layered double hydroxides in biomass valorisation. *Curr. Opin. Green Sustain. Chem.* **2019**, *22*, 29–38. [[CrossRef](#)]
28. Barranca, A.; Gandarias, I.; Arias, P.L.; Agirrezabal-Telleria, I. One-Pot Production of 1, 5-Pentanediol from Furfural Through Tailored Hydrotalcite-Based Catalysts. *Catal. Lett.* **2022**, 1–8. [[CrossRef](#)]
29. Liu, M.; Yuan, L.; Fan, G.; Zheng, L.; Yang, L.; Li, F. NiCu Nanoparticles for Catalytic Hydrogenation of Biomass-Derived Carbonyl Compounds. *ACS Appl. Nano Mater.* **2020**, *3*, 9226–9237. [[CrossRef](#)]
30. Liu, W.; Yang, Y.; Chen, L.; Xu, E.; Xu, J.; Hong, S.; Zhang, X.; Wei, M. Atomically-Ordered Active Sites in NiMo Intermetallic Compound toward Low-Pressure Hydrodeoxygenation of Furfural. *Appl. Catal. B Environ.* **2020**, *282*, 119569. [[CrossRef](#)]
31. Wu, J.; Gao, G.; Li, J.; Sun, P.; Long, X.; Li, F. Efficient and versatile CuNi alloy nanocatalysts for the highly selective hydrogenation of furfural. *Appl. Catal. B Environ.* **2017**, *203*, 227–236. [[CrossRef](#)]

32. Ren, F.; Wang, Z.; Luo, L.; Lu, H.; Zhou, G.; Huang, W.; Hong, X.; Wu, Y.; Li, Y. Utilization of Active Ni to Fabricate Pt-Ni Nanoframe/NiAl Layered Double Hydroxide Multifunctional Catalyst through In Situ Precipitation. *Chem. Eur. J.* **2015**, *21*, 13181–13185. [[CrossRef](#)] [[PubMed](#)]
33. Rao, T.U.; Suchada, S.; Choi, C.; Machida, H.; Huo, Z.; Norinaga, K. Selective hydrogenation of furfural to tetrahydrofurfuryl alcohol in 2-butanol over an equimolar Ni-Cu-Al catalyst prepared by the co-precipitation method. *Energy Convers. Manag.* **2022**, *265*, 115736. [[CrossRef](#)]
34. Yang, K.; Li, Y.; Wang, R.; Li, Q.; Huang, B.; Guo, X.; Zhu, Z.; Su, T.; Lü, H. Synthesis of Dual-Active-Sites Ni-Ni<sub>2</sub>In catalysts for selective hydrogenation of furfural to furfuryl alcohol. *Fuel* **2022**, *325*, 124898. [[CrossRef](#)]
35. Huang, L.; Tang, F.; Liu, P.; Xiong, W.; Jia, S.; Hao, F.; Lv, Y.; Luo, H. Highly efficient and selective conversion of guaiacol to cyclohexanol over Ni-Fe/MgAlO<sub>x</sub>: Understanding the synergistic effect between Ni-Fe alloy and basic sites. *Fuel* **2022**, *327*, 125115. [[CrossRef](#)]
36. Chen, X.; Liu, W.; Luo, J.; Niu, H.; Li, R.; Liang, C. Structure Evolution of Ni-Cu Bimetallic Catalysts Derived from Layered Double Hydroxides for Selective Hydrogenation of Furfural to Tetrahydrofurfuryl Alcohol. *Ind. Eng. Chem. Res.* **2022**, *61*, 12953–12965. [[CrossRef](#)]
37. Shao, Y.; Wang, J.; Sun, K.; Gao, G.; Li, C.; Zhang, L.; Zhang, S.; Xu, L.; Hu, G.; Hu, X. Selective hydrogenation of furfural and its derivative over bimetallic NiFe-based catalysts: Understanding the synergy between Ni sites and Ni-Fe alloy. *Renew. Energ.* **2021**, *170*, 1114–1128. [[CrossRef](#)]
38. Pomeroy, B.; Grilc, M.; Likozar, B. Process condition-based tuneable selective catalysis of hydroxymethylfurfural (HMF) hydrogenation reactions to aromatic, saturated cyclic and linear poly-functional alcohols over Ni-Ce/Al<sub>2</sub>O<sub>3</sub>. *Green Chem.* **2021**, *23*, 7996–8002. [[CrossRef](#)]
39. Theiss, F.L.; Ayoko, G.A.; Frost, R.L. Synthesis of layered double hydroxides containing Mg<sup>2+</sup>, Zn<sup>2+</sup>, Ca<sup>2+</sup> and Al<sup>3+</sup> layer cations by co-precipitation methods—A review. *Appl. Surf. Sci.* **2016**, *383*, 200–213. [[CrossRef](#)]
40. Teodorescu, F.; Slabu, A.I.; Pavel, O.D.; Zăvoianu, R. A comparative study on the catalytic activity of ZnAl, NiAl, and CoAl mixed oxides derived from LDH obtained by mechanochemical method in the synthesis of 2-methylpyrazine. *Catal. Commun.* **2019**, *133*, 105829. [[CrossRef](#)]
41. Stepanova, L.N.; Belskaya, O.B.; Vasilevich, A.V.; Leont'eva, N.N.; Salanov, A.N.; Likholobov, V.A. Synthesis and study of Mg(Ni, Co, Li)Al-LDH prepared by mechanochemical method. *AIP Conf. Proc.* **2019**, *2141*, 020013. [[CrossRef](#)]
42. Stepanova, L.N.; Belskaya, O.B.; Leont'eva, N.N.; Kobzar, E.O.; Salanov, A.N.; Gulyaeva, T.I.; Trenikhin, M.V.; Likholobov, V.A. Study of the Properties of the Catalysts Based on Ni(Mg)Al-Layered Hydroxides for the Reaction of Furfural Hydrogenation. *Mater. Chem. Phys.* **2020**, *263*, 124091. [[CrossRef](#)]
43. Stepanova, L.N.; Kobzar, E.O.; Leont'eva, N.N.; Gulyaeva, T.I.; Vasilevich, A.V.; Babenko, A.V.; Serkova, A.N.; Salanov, A.N.; Belskaya, O.B. Study of the chemical and phase transformations in the mechanochemical synthesis of the MgAl-layered double hydroxide. *J. Alloys Compd.* **2022**, *890*, 161902. [[CrossRef](#)]
44. Belskaya, O.B.; Mironenko, R.M.; Gulyaeva, T.I.; Trenikhin, M.V.; Muromtsev, I.V.; Trubina, S.V.; Zvereva, V.V.; Likholobov, V.A. Catalysts Derived from Nickel-Containing Layered Double Hydroxides for Aqueous-Phase Furfural Hydrogenation. *Catalysts* **2022**, *12*, 598. [[CrossRef](#)]
45. Mironenko, R.M.; Likholobov, V.A.; Belskaya, O.B. Nanoglobular carbon and palladium–nanoglobular carbon catalysts for liquid-phase hydrogenation of organic compounds. *Russ. Chem. Rev.* **2022**, *91*, RCR5017. [[CrossRef](#)]
46. Fan, Q.; Li, X.; Yang, Z.; Han, J.; Xu, S.; Zhang, F. Double-Confined Nickel Nanocatalyst Derived from Layered Double Hydroxide Precursor: Atomic Scale Insight into Microstructure Evolution. *Chem. Mater.* **2016**, *28*, 6296–6304. [[CrossRef](#)]
47. Han, J.; Jia, H.; Yang, Z.; Fan, Q.; Zhang, F. Confined hexahedral nickel nanoparticle catalyst for catalytic hydrogenation reaction. *J. Mater. Sci.* **2017**, *53*, 4884–4896. [[CrossRef](#)]
48. Abello, S.; Verboekend, D.; Bridier, B.; Perezramirez, J. Activated takovite catalysts for partial hydrogenation of ethyne, propyne, and propadiene. *J. Catal.* **2008**, *259*, 85–95. [[CrossRef](#)]
49. Cherepanova, S.V.; Leont'eva, N.N.; Arbuzov, A.B.; Drozdov, V.A.; Belskaya, O.B.; Antonicheva, N.V. Structure of Oxides Prepared by Decomposition of Layered Double Mg–Al and Ni–Al Hydroxides. *J. Solid State Chem.* **2015**, *225*, 417–426. [[CrossRef](#)]
50. Qu, J.; Sha, L.; Wu, C.; Zhang, Q. Applications of Mechanochemically Prepared Layered Double Hydroxides as Adsorbents and Catalysts: A Mini-Review. *Nanomaterials* **2019**, *9*, 80. [[CrossRef](#)]
51. Wu, Z.-Z.; Gao, F.-Y.; Gao, M.-R. Regulating the oxidation state of nanomaterials for electrocatalytic CO<sub>2</sub> reduction. *Energy Environ. Sci.* **2021**, *14*, 1121–1139. [[CrossRef](#)]
52. Zhou, X.; Shan, J.; Chen, L.; Xia, B.Y.; Ling, T.; Duan, J.; Jiao, Y.; Zheng, Y.; Qiao, S.-Z. Stabilizing Cu<sup>2+</sup> ions by solid solutions to promote CO<sub>2</sub> electroreduction to methane. *J. Am. Chem. Soc.* **2022**, *144*, 2079–2084. [[CrossRef](#)] [[PubMed](#)]

**Disclaimer/Publisher's Note:** The statements, opinions and data contained in all publications are solely those of the individual author(s) and contributor(s) and not of MDPI and/or the editor(s). MDPI and/or the editor(s) disclaim responsibility for any injury to people or property resulting from any ideas, methods, instructions or products referred to in the content.